Journal of Solid State Chemistry 182 (2009) 560–565

Contents lists available at ScienceDirect

Journal of Solid State Chemistry

journal homepage: www.elsevier.com/locate/jssc

Structural characterization and photocatalytic activity of hollow binary ZrO_2/TiO_2 oxide fibers

Baochao Wu, Rusheng Yuan *, Xianzhi Fu

Research Institute of Photocatalysis, Chemistry & Chemical Engineering College, Fuzhou University, Fuzhou 350002, China

ARTICLE INFO

Article history:
Received 24 August 2008
Received in revised form
4 November 2008
Accepted 16 November 2008
Available online 6 December 2008

Keywords:
Hollow ZrO_2/TiO_2 fibers
Structure characterization
Photocatalytic activity

ABSTRACT

The formation of hollow binary ZrO_2/TiO_2 oxide fibers using mixed precursor solutions was achieved by activated carbon fibers templating technique combined with solvothermal process. The samples were characterized by scanning electron microscopy (SEM), transmission electron microscopy (TEM), X-ray diffraction (XRD), N_2 adsorption, X-ray photoelectron spectroscopy (XPS), UV–vis, and infrared (IR) spectroscopy. The binary oxide system shows the anatase-type TiO_2 and tetragonal phase of ZrO_2, and the introduction of ZrO_2 notably inhibits the growth of TiO_2 nanocrystallites. Although calcined at 575 °C, all hollow ZrO_2/TiO_2 fibers exhibit higher surface areas ($>113\ m^2/g$) than pure TiO_2 hollow fibers. The Pyridine adsorption on ZrO_2/TiO_2 sample indicates the presence of stronger surface acid sites. Such properties bring about that the binary oxide system possesses higher efficiency and durable activity stability for photodegradation of gaseous ethylene and trichloromethane than *P*25 TiO_2. In addition, the macroscopic felt form for the resulting materials is more beneficial for practical applications than traditional catalysts forms.

© 2008 Elsevier Inc. All rights reserved.

1. Introduction

Titanium dioxide has been widely used as photocatalyst for solar energy conversion and environmental applications (water and air purification) because of relatively high activity, chemical stability, low cost, and nontoxicity. Even so, slow reaction rate and poor solar efficiency have hindered its further applications. In order to enhance its application and photocatalytic property, much attention has been paid in recent years to modify TiO_2 with different methods such as establishing junctions between titania and other semiconductors [1,2], doping with metals or ions [3–5] and composite design with porous materials [6–8]. ZrO_2 is a *n*-type semiconductor with similar physico-chemical properties to TiO_2, and widely used in ceramics technology and heterogeneous catalysis. Many authors prepared TiO_2 doped by ZrO_2 using various methods, such as sol–gel [9,10], polymer gel templating [11], homogeneous co-precipitation [3], and hydrothermal synthesis [12], and higher photocatalytic activity was found in comparison with pure TiO_2. The increase of surface acidity, surface area and oxygen vacancy defects are thought to be responsible for the enhanced activity. However, most of the synthesized ZrO_2/TiO_2 materials are in the forms of powder and film, and there remain some difficulties in field applications. Therefore, it is highly desirable to synthesize ZrO_2/TiO_2 composites with both macroscopic scale and higher photocatalytic activity.

Controlling the morphological properties of materials during synthesis is of great importance, as these structural characteristics strongly influence their performances and purposes. For ZrO_2/TiO_2 system, its catalytic activity is well known to be sensitive to the composition and structural properties. So, in this work, porous structure was introduced to the ZrO_2/TiO_2 binary oxide system to achieve efficient mass transfer. We have proposed a route, activated carbon fibers (ACFs) templating technique combined with solvothermal process, to synthesize pure oxide hollow fibers with hierarchical porous structure in our previous study [13]. Here, this process was extended to construct binary ZrO_2/TiO_2 oxide fibers with both porous structure and macroscopic shape on the centimeter scale. The photocatalytic activities of the synthesized samples were determined by degradation of two organic gaseous molecules: ethylene and trichloromethane. Meanwhile, the correlation between the zirconia content and photocatalytic activity was discussed.

2. Experimental

2.1. Materials preparation

ACFs were produced from rayon precursor, in the form of felt, having a BET surface area of $1000\ m^2/g$ and an average pore size of 0.78 nm. The fibers were pretreated with concentrated nitric acid

* Corresponding author. Fax: +86 591 83779105.
E-mail address: yuanrs2002@yahoo.com.cn (R. Yuan).

0022-4596/$ - see front matter © 2008 Elsevier Inc. All rights reserved.
doi:10.1016/j.jssc.2008.11.030

(65%) for 24 h to remove the surface impurities and create the oxygenated functionalities. After washing with distilled water, the fiber was dried at 423 K in vacuum atmosphere for 10 h. Titanium tetraisopropoxide (TTIP; 99%) and zirconium *n*-propoxide (ZNP; 70%) were purchased from Shanghai Reagent and Aldrich Corporation, respectively. The Degussa *P*25 titania has a surface area of 50 m^2/g and an average particle size of 30 nm. All other reagents (analytical grade) were purchased from Fuchen Chemical Plant and used as received.

A 1 g of the acid-treated ACF was immersed in 60 mL solution containing the mixed precursors (TTIP and ZNP with different volume ratios) and anhydrous ethanol (3:16, V/V). After sonication for 45 min to remove the air in ACF, the autoclave was sealed. All above procedures were carried out inside a glove box to avoid the effect of water molecules. Then the autoclave was heated to 453 K under autogenous pressure for 24 h. When it was cooled down to room temperature, the sample was taken out and rinsed with anhydrous ethanol to remove excessive TTIP and ZNP, and dried at 333 K. Finally, the composite fibers were calcined at the temperature of 848 K (ramp of 1 K/min) in a flow of O_2 (80 mL/min) for 6 h to remove the ACF templates and form mixed oxides crystalline. The volume ratio of TTIP to ZNP was 2, 1.1 and 0.8, and the resultant ZrO_2/TiO_2 composite fibers were denoted as ZT1, ZT2 and ZT3 with a ZrO_2 content of 8.4, 12.6 and 19.7 wt%, respectively. For comparison, pure TiO_2 fibers (T0) were prepared under the identical conditions using TTIP as the precursor.

2.2. Characterization

The morphology of hollow ZrO_2/TiO_2 fibers was determined by scanning electron microscopy (SEM, JEOL JSM-6700F) and

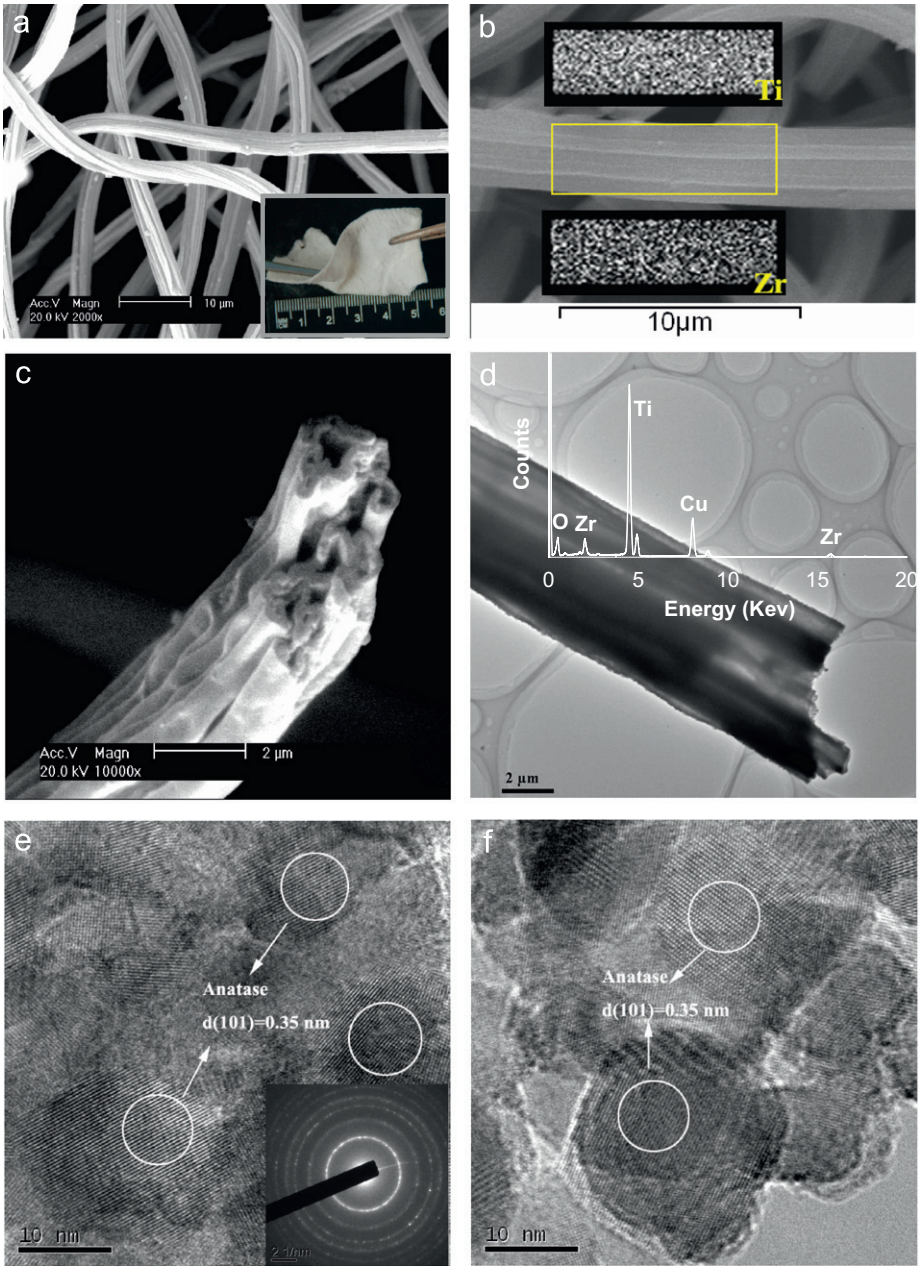

Fig. 1. (a–e) Typical morphologies for ZT3 sample: (a) overview of the ZrO_2/TiO_2 fibers (inset, the photograph of the ZrO_2/TiO_2 fiber felt); (b) elemental mapping patterns of a selected area along the fiber length; (c) broken fiber sections indicating the hollow nature; (d) a low magnitude TEM image and EDX spectrum; (e) high-resolution TEM image for the particles in the ZrO_2/TiO_2 fiber wall (inset, electron diffraction pattern); and (f) the particles in ZT1 fiber wall.

transmission electron microscopy (TEM, JEOL JEM-2010EX) equipped with an energy dispersive X-ray (EDX) analyzer (Phoenix). The X-ray diffraction (XRD) patterns of all samples were collected using a Bruker D8 Advance X-ray diffractometer (Cu$K\alpha$ radiation) at a scanning speed of 2° (2θ)/min in the 2θ range of 10–80°. The BET surface area was obtained by N_2 adsorption at 77 K using a Micromeritics ASAP 2020. The pore size distribution was calculated by using the BJH model. UV–vis reflectance measurement was made using a RSA-MR-30 reflectance spectroscopy accessory (Labsphere Inc., North Sutton, NH) attached to a Milton Roy Spectronic 3000 diode array spectrophotometer (Milton Roy, San Leandro, CA). X-ray photoelectron spectroscopy (XPS) spectra were recorded on a PHI Quantum 2000 XPS system with a monochromatic Al$K\alpha$ X-ray source and a charge neutralizer. The ZrO_2 content of the obtained composite fibers was determined by inductively coupled plasma atomic emission spectrometry (ICP-AES, Plasma 300). In situ FT-IR spectra were performed on a Nicolet Nexus 670 FT-IR spectrometer at a resolution of 4 cm^{-1}. The sample was pressed into a self-supporting thin wafer and put into the sample holder. The wafer was degassed in dynamic vacuum (10^{-2} Pa) at 573 K for 3 h, and then the background spectrum was recorded. After equilibrium of adsorption of pyridine vapor for 1 h, the spectrum was recorded after degassing the wafer under vacuum at 393 K for 2 h.

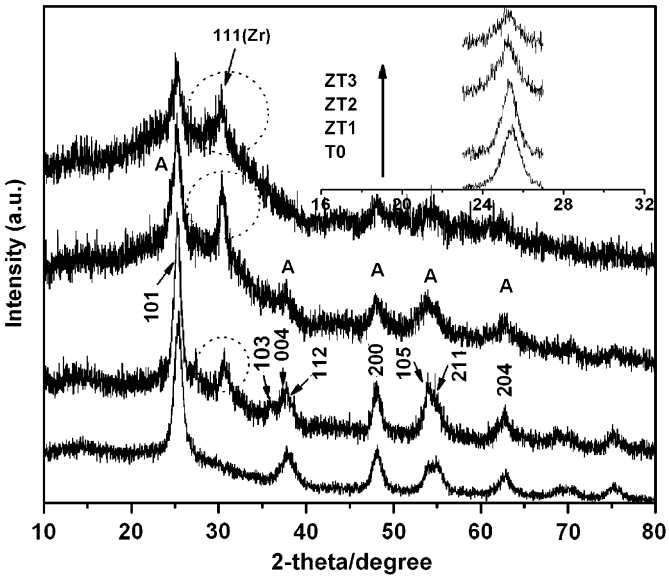

Fig. 2. XRD patterns of three ZrO_2/TiO_2 composite fibers and pure TiO_2 fibers.

2.3. Photocatalytic experiment

A total of 60 mg catalyst was packed into a Pyrex tubular reactor with 8 cm filling length and 4 mm inner diameter. In all cases, the amount of the catalyst and the illuminated length were identical. For ethylene photodegradation, illumination was provided by four 8-W UV lamps with a major emission at 365 nm. Prior to the experiments, the catalyst was allowed to reach adsorption equilibrium. Ethylene diluted in zero air (21% O_2 and 79% N_2) was used to afford a reactant stream (flow rate: 20 mL/min), and the initial concentration of ethylene was 90 ppm. The concentrations of residual ethylene and the produced

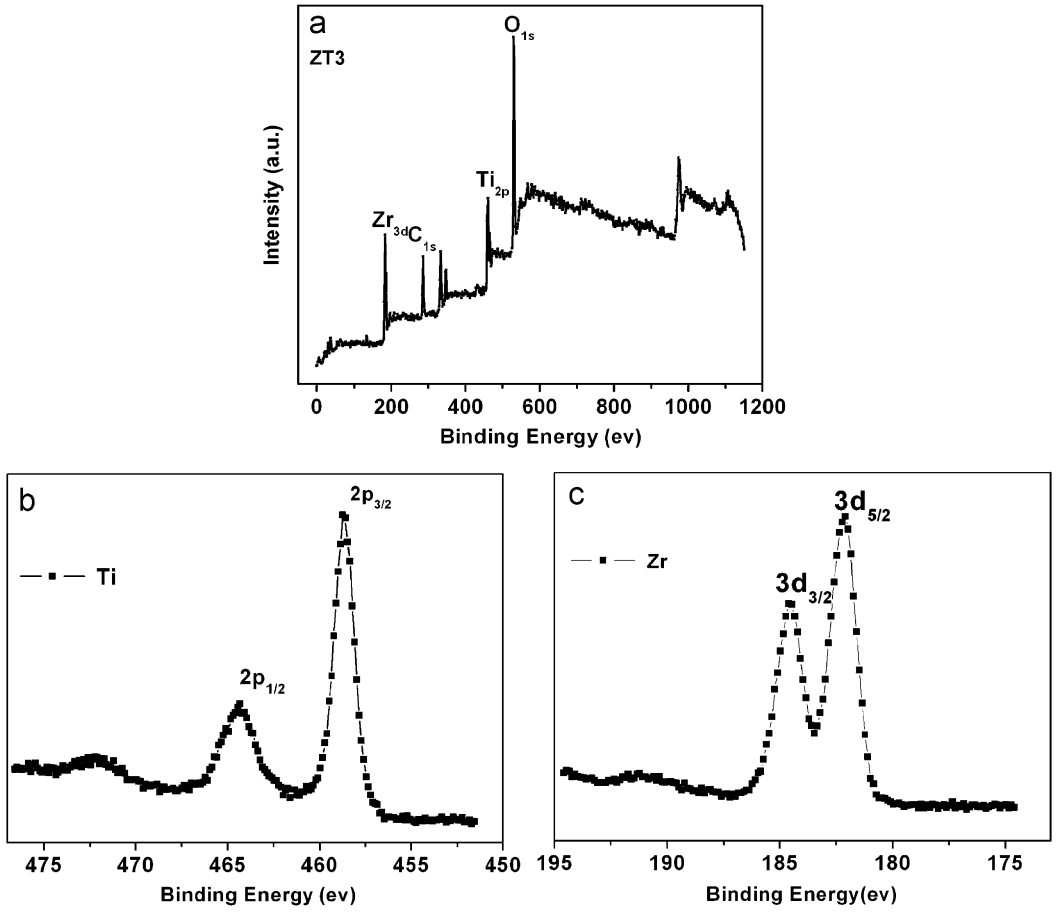

Fig. 3. (a) Survey XPS spectrum of ZT3; (b and c) high-resolution spectrum of Ti2*p* and Zr3*d*, respectively.

CO_2 were measured by gas chromatography (GC, Hewlett-Packard 4890), equipped with Porapak R column, a flame ionization detector (FID) and a thermal conductivity detector (TCD). In the case of trichloromethane, four 8-W UV lamps (with major emission at 254 nm) were used for irradiation. The initial concentration was 57 ppm with a flow rate of 20 mL/min.

3. Results and discussion

ACF is a kind of porous adsorption materials with a diameter of 10 μm, and possesses a plenty of surface functional groups (especially hydroxyl) after HNO_3 oxidation. Strong adsorption allows that the precursors were quickly adsorbed and then reacted with such functional groups as well as residual trace-water molecules on ACF, resulting in sufficient nanoparticles deposition on the walls of the fiber so that removal of ACF template gave fibrous ZrO_2/TiO_2 structure. Fig. 1a shows the typical morphology of ZT3 sample. The ZrO_2/TiO_2 fibers are highly dispersed without any aggregation between each other, with a large length on the centimeter scale and an average diameter of 4 μm. The macroscopic products are in the form of textile (inset, Fig. 1a) and possess a certain strength and flexibleness, allowing easier manipulation in applications. A higher magnification SEM image of individual fiber (Fig. 1b) shows that its surface is full of groove and ridge structure along the length direction, inherited from the original template fiber. From the broken section of ZrO_2/TiO_2 fiber (Fig. 1c), we can observe that a multi-channel hollow structure with a mean wall thickness of 260 nm although the calcination process caused the partial collapse and shrinkage of hollow framework. This hollow nature is also confirmed by TEM, as shown in Fig. 1d.

The micrograph of high magnification TEM (Fig. 1e) depicts the ZrO_2/TiO_2 fiber (ZT3) wall consists of 15 nm particles with lattice fringes of 0.35 nm, which can be indexed to the (101) crystallographic planes for anatase-TiO_2. This may be further corroborated by the electron diffraction pattern (inset, Fig. 1e) of these particles, which shows several weak Debye–Scherrer rings, corresponding to the reflections of the polycrystalline anatase phase. For ZT1 sample with the lowest ZrO_2 content, the size of anatase-TiO_2 particle increases to about 20 nm, as shown in Fig. 1f. Although the ZrO_2 particles cannot be discerned from the images, the EDX spectrum (inset, Fig. 1d) of a selected area on ZrO_2/TiO_2 fiber shows that the fiber consists of titanium, zirconium and oxygen atoms. Moreover, both Ti and Zr atoms are uniformly dispersed in the fiber wall, as seen from the element mapping pattern of the selected area on the fiber surface (Fig. 1b).

The wide-angle XRD patterns of three ZrO_2/TiO_2 fibers with various ZrO_2 contents are shown in Fig. 2. It can be clearly observed that several stronger diffraction peaks assigned to the anatase phase of TiO_2, and a small diffraction peak at 30° corresponding to the ZrO_2 tetragonal phase appear for all ZrO_2/TiO_2 samples. Thus, the incorporation of ZrO_2 does not lead to a solid solution. With the increase of ZrO_2 content, the diffraction peaks of TiO_2 become much weaker and wider gradually, which means ZT3 with a smallest crystal size for TiO_2. This also indicates that the presence of the second component (ZrO_2) in sufficient amount notably inhibits the growth of TiO_2 nanocrystallites.

Further information about the surface electronic structure as well as the chemical valence of the products can be provided by XPS spectra. Fig. 3 shows the XPS spectra of ZT3. The survey XPS spectrum (Fig. 3a) reveals the surface of ZrO_2/TiO_2 binary oxide fiber is composed of Ti, Zr and O atoms, consistent with the EDX result. The high-resolution Ti 2*p* spectrum (Fig. 3b) shows two distinct peaks at binding energies of 458.6 and 464.4 eV for

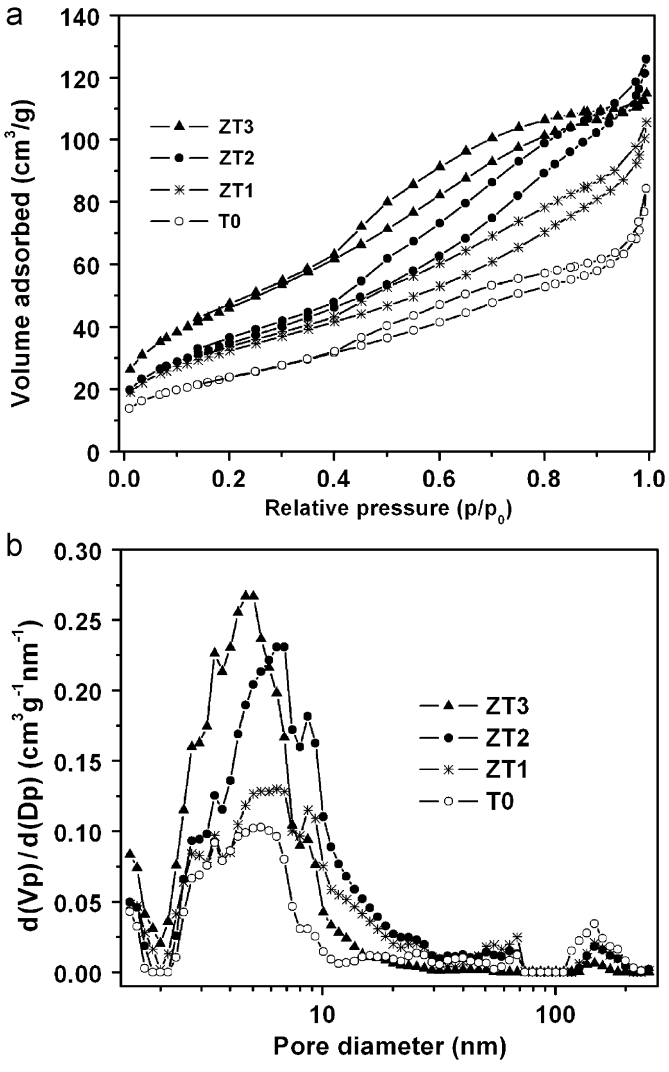

Fig. 4. (a and b) N_2 adsorption–desorption isotherms and corresponding pore size distributions for three ZrO_2/TiO_2 fibers and pure TiO_2 fibers.

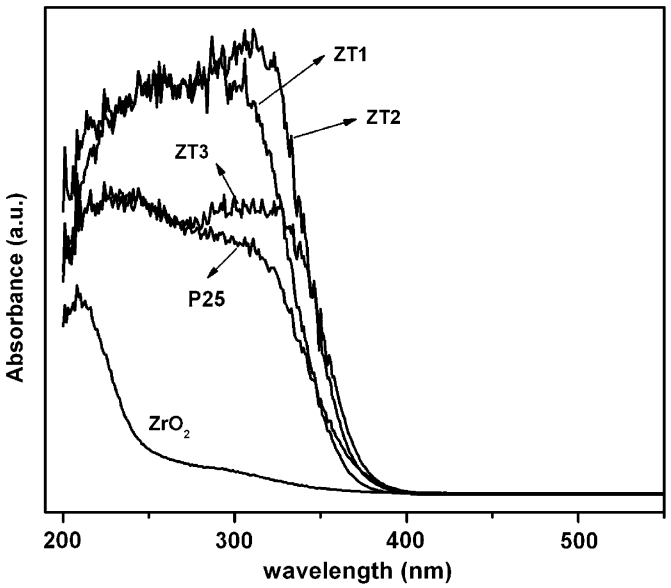

Fig. 5. UV–vis diffuse reflectance spectra of three ZrO_2/TiO_2 samples and *P*25.

Ti $2p_{3/2}$ and Ti $2p_{1/2}$, respectively, in good agreement with the values reported for TiO_2 in the literature [14]. The Zr $3d_{5/2}$ and Zr $3d_{3/2}$ binding energies values are 182.2 and 184.7 eV, corresponding to an oxidation state of 4+ in ZrO_2 [15]. These results further corroborate the presence of TiO_2 and ZrO_2 only in the synthesized composite fibers.

Nitrogen adsorption isotherms and corresponding pore size distributions for three ZrO_2/TiO_2 samples are shown in Fig. 4. All isotherms (Fig. 4a) exhibit stepwise adsorption and desorption (type IV isotherms), indicative of a typical mesoporous structure. The corresponding pore size distribution plots (Fig. 4b) display that all ZrO_2/TiO_2 samples possess dominantly mesopores in addition to small amount of micropores and macropores. The ZT3 sample has a mean pore diameter of ~4.2 nm, slightly smaller than other two samples, resulting in it with the highest specific surface area of 166 m^2/g. Although calcination at 575 °C, the surface areas of three samples (113 and 125 m^2/g for ZT1 and ZT2, respectively) are all higher than that of pure TiO_2 hollow fiber (83 m^2/g) prepared under the same conditions, suggesting that the addition of ZrO_2 can increase the specific surface area due to the preservation of interconnected porous networks in the binary oxide system.

Fig. 5 shows the UV–vis diffuse reflectance spectra of three ZrO_2/TiO_2 samples and *P*25. For all binary oxides samples, a slight shift toward longer wavelength in absorption band is detected. This is probably due to the fact that the enhanced concentration of the oxygen vacancies in binary oxides system forms a defect band that further changes the energy of conduction band [3]. However, the addition of ZrO_2 does not alter so much absorption edge of the binary oxides system, and they are still concentrated at ~390 nm, close to that of *P*25.

The photocatalytic activity of the hollow ZrO_2/TiO_2 fibers were investigated and compared with a reference photocatalyst (Degussa *P*25 titania) using ethylene and trichloromethane photodegradation as the test reactions. Fig. 6a shows the photocatalytic activity of the synthesized ZrO_2/TiO_2 fibers and *P*25 for ethylene. All ZrO_2/TiO_2 samples exhibit higher activity toward ethylene photodegradation than the Degussa *P*25 photocatalyst. It is also found that the ZrO_2 content in composite system affects the photocatalytic activity of the ZrO_2/TiO_2 fibers. The activity of ZrO_2/TiO_2 increases gradually with increasing ZrO_2 content. When the ZrO_2 content of 19.7 wt%, the ZrO_2/TiO_2 fibers (ZT3) possess highest photocatalytic activity, reaching an efficiency of 136% of the *P*25. It should be mentioned that the photocatalytic activity of the composite system would decrease when the ZrO_2 content amounts to a critical value because pure ZrO_2 is not a photocatalyst under the illumination used.

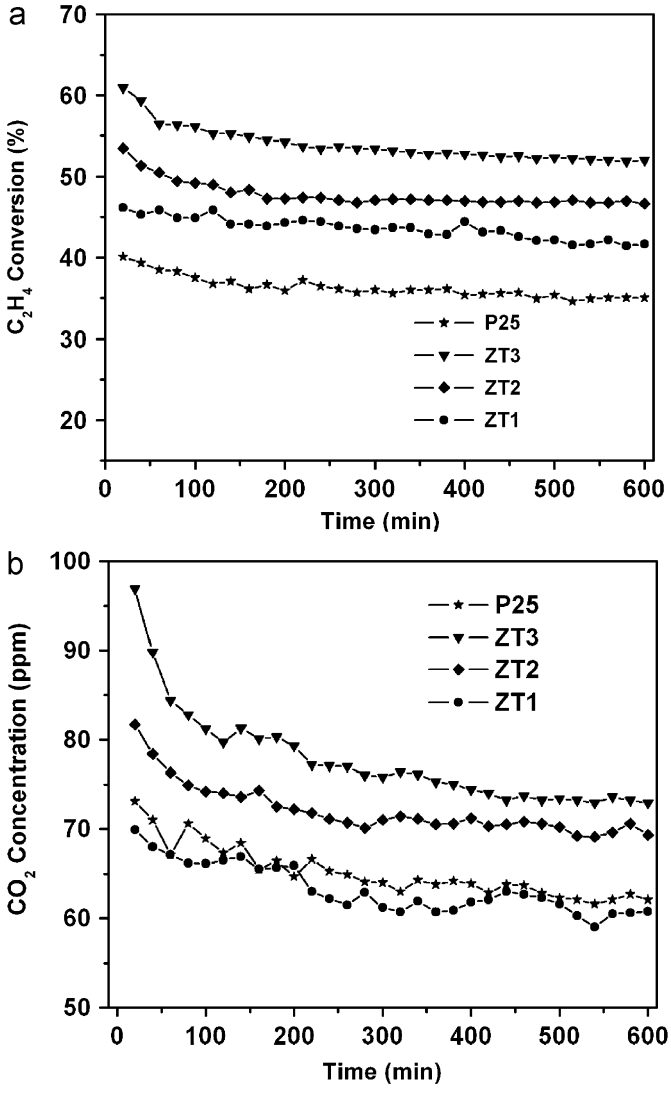

Fig. 6. (a) Photocatalytic conversion of ethylene over three ZrO_2/TiO_2 samples and *P*25 and (b) the corresponding CO_2 yield with time under UV irradiation.

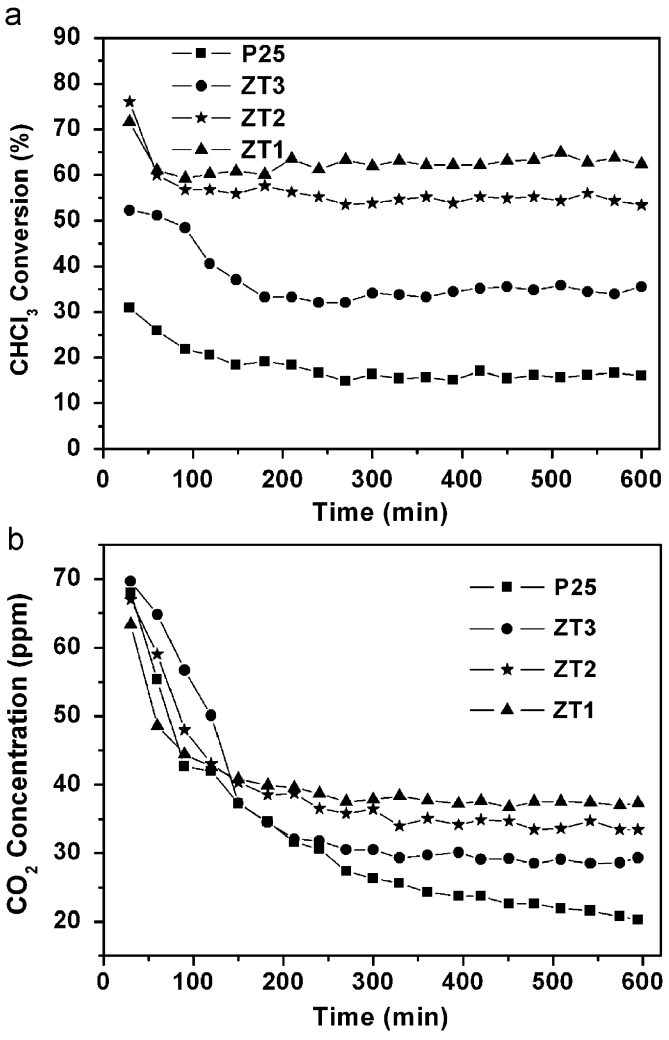

Fig. 7. (a) Photocatalytic degradation of trichloromethane by three ZrO_2/TiO_2 samples and *P*25 and (b) the corresponding CO_2 yield versus time.

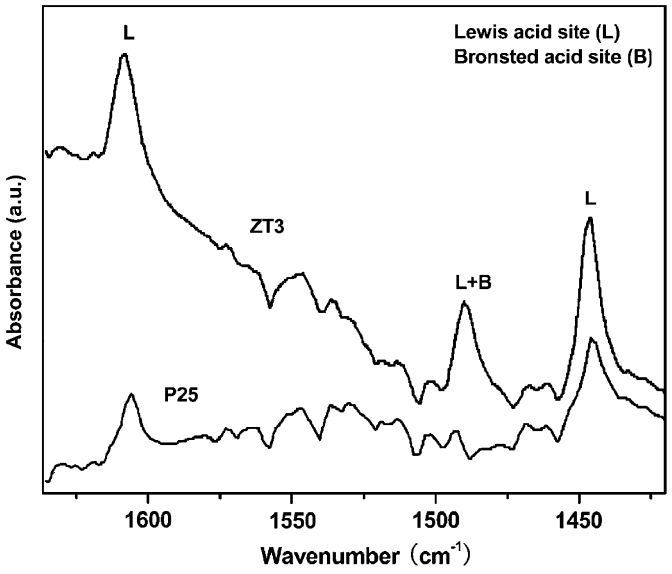

Fig. 8. Infrared spectra of pyridine molecules chemisorbed on ZT3 and *P*25.

Although the conversion rate of ethylene on this sample decreases slightly at the beginning, it stabilizes after 3 h and keeps at about 52% after 10 h. This degradation efficiency is very high because small amount of catalyst (about 60 mg) was used in our experiment, far less than the catalyst amount used by others [9,16]. The measurement of CO_2 (Fig. 6b) produced from the reaction also confirms the beneficial effect of ZrO_2 incorporation.

Halogenated hydrocarbons are the most frequent and toxic chemical contaminants in a wide range of environments, so we selected trichloromethane to test the performance of the ZrO_2/TiO_2 composite catalyst. Fig. 7a shows the photodecomposition of trichloromethane over the prepared ZrO_2/TiO_2 fibers and *P*25. All ZrO_2/TiO_2 fibers present better photocatalytic activity than *P*25, but highest efficiency (about 387% of the *P*25) is obtained by ZT1 sample, unlike the case for ethylene. This means that Ti/Zr ratio in ZrO_2/TiO_2 fibers has a different influence on diverse molecules when photodegradation, possibly due to the oxidation process via a dissimilar reaction mechanism. Carbon dioxide is formed during $CHCl_3$ degradation, as shown in Fig. 7b. The concentrations of CO_2 for three ZrO_2/TiO_2 samples maintain stable after 3 h, whereas that for *P*25 decreases gradually. This result suggests that ZrO_2/TiO_2 fibers have better mineralization efficiency and activity stability than *P*25.

The composite ZrO_2/TiO_2 system was found to exhibit excellent efficiency for both ethylene and trichloromethane degradation. Its better performance can be mainly attributed to high specific surface area, porous structure and nature of surface groups. The large surface area provides more surface sites for the adsorption of reactants molecules, making the photocatalytic process more efficient. The interconnected porous networks favor diffusion of the reactant molecules into the catalyst. Another reason is zirconia modified titania with higher surface acidity. As shown in Fig. 8, the spectrum of ZT3 contains several significant peaks at 1445, 1489, and 1607 cm^{-1}. These peaks can be assigned to the chemisorption of molecular pyridine at surface acidic sites (mainly Lewis acidic sites) [17,18]. In the case of *P*25, only small peaks corresponding to pyridine adsorbed on Lewis acidic sites are observed, suggesting it with weak surface acidities. Such surface sites with higher acidity may prove to be better adsorption sites or hole traps. In addition, anatase-type TiO_2 together with relatively smaller crystal size caused by the presence of ZrO_2 is also responsible for the improvement in the photocatalytic activity of the composite system.

4. Conclusions

Hollow binary ZrO_2/TiO_2 fibers with different ZrO_2 contents were successfully constructed by ACFs templating technique combined with solvothermal process. The introduction of ZrO_2 endows the resulting composite fibers with high surface area, increased surface acidity and relatively smaller crystal size. All these factors lead to an excellent efficiency and durable activity stability for photodegradation of typical air pollutants (ethylene and trichloromethane) than Degussa *P*25. Furthermore, the final products are in the form of felt, which can be manipulated more easily in practical applications than the forms of powder and film. Also, this study offers some new insight into designing high efficient catalysts with the desired structural features for environmental remediation.

Acknowledgments

This work was financially supported by the National Nature Science Foundation of China (no. 20701008), the Natural Science Foundation of Fujian Province of China (no. E0610011), the Key Project of Chinese Ministry of Education (no. 207053), and the National Basic Research Program of China (973 Program: 2007CB613306).

References

[1] M.D. Hernández-Alonso, I. Tejedor-Tejedor, J.M. Coronado, J. Soria, M.A. Anderson, Thin Solid Film 502 (2006) 125–131.
[2] J. Aguado, R. van Grieken, M.-J. López-Muñoz, J. Marugán, Appl. Catal. A: Gen. 312 (2006) 202–212.
[3] J. Lukáč, M. Klementová, P. Bezdička, S. Bakardjieva, J. Šubrt, L. Szatmáry, Z. Bastl, J. Jirkovský, Appl. Catal. B: Environ. 74 (2007) 83–91.
[4] Y.M. Wang, S.W. Liu, M.K. Lü, S.F. Wang, F. Gu, X.Z. Gai, X.P. Cui, J. Pan, J. Mol. Catal. A: Chem. 215 (2004) 137–142.
[5] I. Djerdj, D. Arčon, Z. Jagličić, M. Niederberger, J. Solid State Chem. 181 (2008) 1571–1581.
[6] S. Anandan, M. Yoon, J. Photochem. Photobiol. C: Photochem. 4 (2003) 5–18.
[7] A. Jitianu, T. Cacciaguerra, R. Benoit, S. Delpeux, F. Béguin, S. Bonnamy, Carbon 42 (2004) 1147–1151.
[8] T. Torimoto, Y. Okawa, N. Takeda, H. Yoneyama, J. Photochem. Photobiol. A: Photochem. 103 (1997) 153–157.
[9] X.Z. Fu, L.A. Clark, Q. Yang, M.A. Anderson, Environ. Sci. Technol. 30 (1996) 647–653.
[10] G. Colón, M.C. Hidalgo, J.A. Navío, Appl. Catal. A: Gen. 231 (2002) 185–199.
[11] J.H. Schattka, D.G. Shchukin, J. Jia, M. Antonietti, R.A. Caruso, Chem. Mater. 14 (2002) 5103–5108.
[12] M. Hirano, C. Nakahara, K. Ota, O. Tanaike, M. Inagaki, J. Solid State Chem. 170 (2003) 39–47.
[13] R. Yuan, X. Fu, X. Wang, P. Liu, L. Wu, Y. Xu, X. Wang, Z. Wang, Chem. Mater. 18 (2006) 4700–4705.
[14] I.-H. Tseng, W.-C. Chang, J.C.S. Wu, Appl. Catal. B: Environ. 37 (2002) 37–48.
[15] K.V.R. Chary, G.V. Sagar, D. Naresh, K.K. Seela, B. Sridhar, J. Phys. Chem. B 109 (2005) 9437–9444.
[16] X. Wang, J.C. Yu, C. Ho, Y. Hou, X. Fu, Langmuir 21 (2005) 2552–2559.
[17] O.M. Busch, W. Brijoux, S. Thomson, F. Schuth, J. Catal. 222 (2004) 174–179.
[18] B.H. Davis, R.A. Keogh, S. Alerasool, D.J. Zalewski, D.E. Day, P.K. Doolin, J. Catal. 183 (1999) 45–52.